The European Journal of Biomedical and Life Sciences 2025, No 4
ISSN 2310-5674

PREMIER Publishing
ppublishing.org

Section 1. Preventive medicine

DOI: 10.29013/EJBLS-25-4-3-18

DISCOVERY OF SMALL MOLECULE INHIBITORS OF MAO-B FOR ALZHEIMER'S DISEASE USING PHARMACOPHORE-BASED VIRTUAL SCREENING

Rory Hu [1]

[1] Groton School, 282 Farmers Row, Groton, Massachusetts, US

Cite: *Rory Hu (2025). Discovery of small molecule inhibitors of MAO-B for Alzheimer's disease using pharmacophore-based virtual screening. The European Journal of Biomedical and Life Sciences 2025, No. 4.* https://doi.org/10.29013/EJBLS-25-4-3-18

Abstract

Effective therapies are needed to mitigate Alzheimer's disease (AD), a neurodegenerative dementia that harms cognitive function in over 10% of people older than 65. Although monoamine oxidase B (MAO-B) is a critical therapeutic target for AD, only three MAO-B inhibitors (rasagiline, selegiline, and safinamide) are currently approved, and they are mainly used for treating Parkinson's Disease. To identify novel MAO-B inhibitors as treatments for AD, *in silico* drug discovery was employed as a cost-effective and efficient approach for screening a vast chemical space. Geometric, energetic, and machine learning methods were used to evaluate potential binding sites, which were subsequently assessed with molecular docking for 20 potential MAO-B inhibitors identified from pharmacophore mapping. These 20 molecules were then analyzed for their pharmacokinetic and toxicological properties via ADMET prediction, and Z56776036 and Z1980993192 were selected as the two most promising drug candidates. These lead compounds had high binding affinity (docking scores below –9 kcal/mol), strong ADME profiles, and low toxicity (LD50 values above 1000 mg/kg). This experiment proposes an innovative method of MAO-B inhibitor discovery. It represents a promising starting point for future work focused on further testing of the 2 lead compounds through *in vitro* screening and additional *in silico* discovery of lead compounds using the methodology of this project.
Keywords: *Alzheimer's disease, monoamine oxidase B, pharmacophore mapping, molecular docking, ADMET prediction, drug discovery*

Introduction

Alzheimer's disease (AD), a type of neurodegenerative dementia, impacts memory and cognitive abilities in over 57 million people worldwide alongside other dementias (*The Lancet*, 2022). It is estimated that 1 in 9 people over the age of 65 have Alzheimer's, and researchers predict that over 152 million people worldwide will have dementia by 2050 (*The Lancet*, 2022; Alzheimer's Associ-

ation, 2024). Additionally, healthcare costs for AD patients are projected to reach almost $1 trillion in 2050 (Alzheimer's Association, 2024). Therefore, treating AD remains a significant concern both for public health and economic stability.

Current FDA-approved drugs for AD include acetylcholinesterase inhibitors (AChEIs), NMDA receptor antagonists, and monoclonal antibodies targeting Aβ proteins (Zhang et al., 2024). AChEIs, such as donepezil, galantamine, and rivastigmine, are the main type of pharmacological treatment for AD (Zuliani et al., 2024). Although they mildly mitigate cognitive decline, AChEIs remain mostly symptomatic (Zuliani et al., 2024). Memantine, the only NMDA receptor antagonist currently approved for AD treatment, is prescribed for patients with moderate to severe AD (Balázs et al., 2021). Usually a second-line treatment after AChEIs, memantine has a small benefit in moderate to severe AD, but not in mild AD (Balázs et al., 2021). Finally, newer drugs for Aβ proteins include aducanumab, lecanemab, and donanemab (Ebell et al., 2024). Cognitive benefits are statistically significant but small, and risks such as edema or hemorrhage remain prevalent with these drugs (Ebell et al., 2024). As a result, many monoclonal antibodies for AD have been discontinued due to their side effects. Since current AD treatments have many drawbacks, researchers have been exploring more promising pathways for AD to develop new drugs.

Two main pathways for AD are the amyloid-β (Aβ) pathway and the neuroinflammation pathway, which have gained more attention in recent years over older pathways such as the cholinergic hypothesis. The amyloidogenic pathway occurs when β-secretase cleaves the amyloid precursor protein (APP) instead of α-secretase, forming soluble APP-β and a C-terminal fragment (CTFβ) instead of soluble APP-α (Hampel et al., 2021). As a result, Aβ peptides are produced, and they clump together in extracellular Aβ plaques that cause aberrant signaling between neurons (Hampel et al., 2021). Additionally, the amyloidogenic pathway can lead to tau hyperphosphorylation, which causes neurofibrillary tangles that are correlated with cognitive decline (Hampel et al., 2021). The neuroinflammation pathway involves the activation of microglia and astrocytes, which lead to inflammatory signaling with neurotoxic effects (Liew et al., 2023). Positive feedback loops as well as Aβ or tau buildup contribute to neuroinflammation, either through further glial activation or increased Aβ accumulation via RIPK1 kinase (Liew et al., 2023; Doig, 2018).

Monoamine oxidase B (MAO-B) can offer insights into new AD treatment through the Aβ and neuroinflammation pathways. MAO-B is an enzyme that breaks down monoamine neurotransmitters such as serotonin, dopamine, and norepinephrine, which regulate mood, cognition, and behavior (Behl et al., 2021). MAO-B works by removing the amino group of the neurotransmitter and oxidizing it, producing an inactive metabolite, an aldehyde (R-CHO), ammonia (NH_3), and hydrogen peroxide (H_2O_2) as a byproduct (Behl et al., 2021). Normally, MAO-B controls mood and motor activity, acting as a metabolic barricade against amines. However, the overexpression of MAO-B enzymes can lead to oxidative stress due to H_2O_2 buildup, causing Aβ plaques and neurofibrillary tangles (Behl et al., 2021). High levels of MAO-B, which breaks down non-hydroxylated amines, are found in astrocytes surrounding Aβ plaques (Behl et al., 2021). The oxidative stress caused by MAO-B overactivity may lead to the Aβ and tau pathways by triggering neuroinflammation, potentially causing Aβ plaques or neurofibrillary tangles.

Because MAO-B is linked to two key pathways for Alzheimer's disease, monoamine oxidase inhibitors (MAOIs), an early class of antidepressants, are being explored as a promising new form of AD treatment. In Alzheimer's disease, the glutamate-GABA balance is disrupted, causing oxidative stress, and MAOIs can restore that balance by increasing GABA levels (Behl et al., 2021). MAOIs also sequester aldehydes and inhibit primary amine oxidase (PrAO), an enzyme that also produces aldehydes promoting Aβ plaque formation (Behl et al., 2021). These mechanisms indicate that MAOIs may be able to reduce oxidative stress in the brain, making them a powerful candidate for early AD treatment.

Researchers have explored various methods for developing MAOI-based AD treatment.

A study by Da Costa et al. used *in silico* preclinical screening to identify 4 lead compounds as potential MAO-B inhibitors, although these compounds have yet to undergo further testing (2024). Additionally, some propargylamines, such as selegiline and rasagiline, can be used as irreversible MAO-B inhibitors by binding covalently to the coenzyme flavin adenine dinucleotide (FAD), permanently disabling MAO-B (Chatzipieris et al., 2024). Newer compounds with internal alkynes are being explored as a way to avoid unwanted side effects of irreversible inhibition, such as upregulation of the GABA-synthesizing enzyme diamine oxidase (DAO) (Chatzipieris et al., 2024). Park et al. developed KDS2010 in 2019, a MAO-B inhibitor that is both reversible and highly selective (2019). By testing on APP/PS1 mice, the researchers discovered that KDS2010 reduces astrocytic GABA levels, bypassing the challenges of selegiline increasing DAO activity (Park et al., 2019). Beyond inhibitors for MAO-B alone, studies have also developed potential AD treatments involving drugs aimed at more than one target. Through *in silico* and *in vitro* analysis, Svobodova et al. tested 24 N-methylpropargylamino-quinazoline derivatives as multi-target directed ligands (MTDLs) for cholinesterases, monoamine oxidases, and N-methyl-D-aspartate receptors (NMDARs) in AD (2023). However, MTDLs face the challenge of selectivity, as they are designed to inhibit more than one enzyme. The potential of MAO-B inhibitors still remains largely unexplored, and no MAO-B inhibitors have passed clinical trials as of 2025. This research aims to improve upon existing work for MAO-B inhibitor discovery and focus on systematic pharmacophore-based *in silico* screening, which is cost-effective and offers rapid results.

Methodology

Figure 1. *Overview of methodology with 5 main steps*

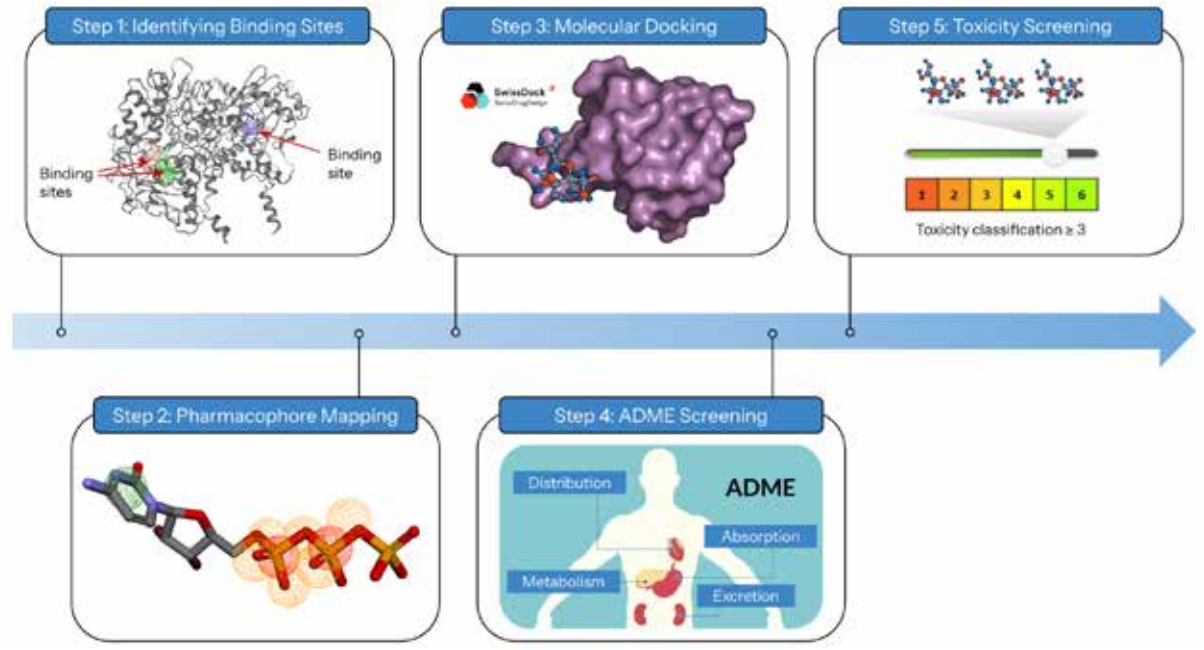

MAO-B Binding Sites

To detect potential binding sites on the MAO-B protein that are both geometrically and energetically viable, computational tools such as DoGSiteScorer, FTSite, and P2Rank were used. DoGSiteScorer detects binding pockets, identifies their geometric and physicochemical properties, and predicts protein druggability to assign a drug score using a support vector machine (Volkamer et al., 2012). MAO-B's PDB code, 6FWC, was applied for DoGSiteScorer on https://proteins.plus/ with default settings (Reis et al., 2018). The "DoGSiteScorer" tab was selected on the website, and all settings were left as default. FTSite uses molecular probes to determine energetically favorable binding sites, as locations where the probes bind are more likely

to be optimal binding sites for ligands (Ngan et al., 2011). Code 6FWC was used on FTSite (https://ftsite.bu.edu/) with default settings. P2Rank uses machine learning to classify Solvent Accessible Surface points, which are regularly spaced points that encode geometric and physicochemical properties (Krivák & Hoksza, 2018). Code 6FWC was inputted on P2Rank with default settings on PrankWeb (https://prankweb.cz/) (Jendele et al., 2019).

Pharmacophore Mapping

Pharmit (https://pharmit.csb.pitt.edu/) was used to generate a pharmacophore map and virtually screen small molecules to match the map (Sunseri & Koes, 2016). Pharmit filters through large drug databases and ranks results via energy minimization (Sunseri & Koes, 2016). To perform virtual screening with pharmacophore mapping in Pharmit, PDB code 6FWC was entered, "FAD" was selected from the adjacent dropdown menu, binding site waters were ignored, and the Enamine database was used. Pharmacophoric features of MAO-B were selected in areas likely to be optimal binding sites, creating 3 maps that captured different areas of the MAO-B enzyme (see Figure 8). Pharmit scanned the Enamine database and produced a list of molecules that matched the pharmacophore maps, from which 20 molecules were selected that had the least root mean square deviation.

Molecular Docking

After identifying the 20 top compounds from the Enamine database, molecular docking with SwissDock was used to test the ability of these compounds to dock on MAO-B (Grosdidier et al., 2011; Bugnon et al., 2024). On swissdock.ch, docking with attractive cavities was used with the SMILES code from Enamine (enaminestore.com) as the ligand and code 6FWC as the target. Chain B of the MAO-B enzyme was selected, and none of the heteroatoms were kept. Chain B was chosen because FTSite detected more potential binding sites on Chain B than Chain A. The search space was then defined with box center (20Å, 128Å, 18Å) and box size (15Å, 17Å, 27Å), as shown in Figure 2. The process was repeated for all 20 compounds.

Figure 2. *Setup of the SwissDock molecular docking. The purple ribbon represents chain B of the MAO-B protein, while the box represents the area where docking was simulated*

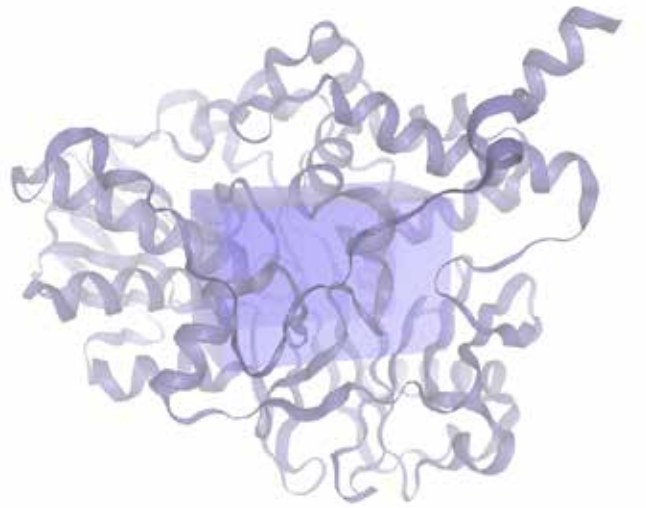

ADME Screening

Based on the results of the molecular docking, the top 10 drug candidates were chosen by most negative SwissParam score. SwissADME was used to determine various physicochemical features for the 10 compounds, as it identified their absorption, distribution, metabolism, and excretion (ADME) capabilities in the human body (Daina et al., 2017). To perform screening with SwissADME, the SMILES code obtained from the Enamine database was entered at http://www.swissadme.ch/. The molecular weight, number of hydrogen bond acceptors, number of hy-

drogen bond donors, and consensus LogP value was used for each drug candidate to determine whether the compound satisfied Lipinski's Rule of Five. Finally, the water solubility (Insoluble < Poorly < Moderately < Soluble < Very < Highly), gastrointestinal (GI) absorption classification, and blood-brain barrier (BBB) permeability were evaluated for each compound. For the screening, the consensus LogP value was used instead of the iLogP value, because the iLogP value was often an outlier from the other calculated LogP values. The ESOL Log S value was used for water solubility. Through this analysis, the number of drug candidates was narrowed down from 10 to 7.

Toxicity Screening

After the ADME screening, toxicity screening was performed on the 7 remaining compounds using ProTox 3.0 (https://tox.charite.de/protox3/). Tox Prediction was selected and the SMILES from the Enamine database was pasted in. All fields in the model prediction box were checked before starting the prediction. Only compounds that had an LD50 value greater than 400 mg/kg and a toxicity classification above 3 were kept, which narrowed the number of compounds down from 7 to 3. Then, examining the network and toxicity radar charts determined the final 2 safest potential candidates.

Results and Discussion

MAO-B Binding Sites

In order to determine potential drug candidates, binding sites on the protein that drugs could bond to were detected. A geometric method (DoGSiteScorer), an energetic method (FTSite), and a machine learning method (P2Rank) were used to predict potential binding sites on the MAO-B protein. DoGSiteScorer, the geometric method, was able to detect 38 potential binding sites. Table 1 shows all of the sites that had a drug score ≥ 0.5, of which there were 17. Two sites, P_0 and P_1, were noticeably larger than the others, although a smaller site (P_5) was ranked first by drug score.

Table 1. *The top 17 binding sites detected by DoGSiteScorer that had drug score ≥ 0.5, sorted by drug score*

Name	Volume (Å³)	Surface Area (Å²)	Drug Score
P_5	411.14	396.08	0.87
P_0	2077.85	1722.15	0.81
P_1	2042.91	1725.6	0.81
P_2	553.72	721.08	0.81
P_3	548.35	748.07	0.79
P_4	460.78	845.28	0.74
P_9	298.12	385.62	0.73
P_11	293.54	173.93	0.72
P_6	370.36	672.77	0.67
P_7	308.87	381.52	0.67
P_10	294.01	326.82	0.65
P_8	306.82	585.96	0.63
P_14	269.67	420.62	0.56
P_12	290.38	514.82	0.54
P_13	277.1	520.46	0.51
P_15	260.66	345.48	0.51
P_20	162.97	247.66	0.5

As seen in Figures 3 and 4, P_0 (yellow) and P_1 (purple) are much larger than the other binding sites. Figure 3 shows the top 3 binding sites, including P_0 and P_1 as well as P_5, which is much smaller but has the highest drug score assigned by DoGSiteScorer. Figure 4 shows all 17 potential binding sites.

Figure 3. *Top 3 binding sites identified by DoGSiteScorer. The red and blue ribbons represent the protein structure, while the green, yellow, and purple represent the binding sites (P_5, P_0, and P_1 respectively)*

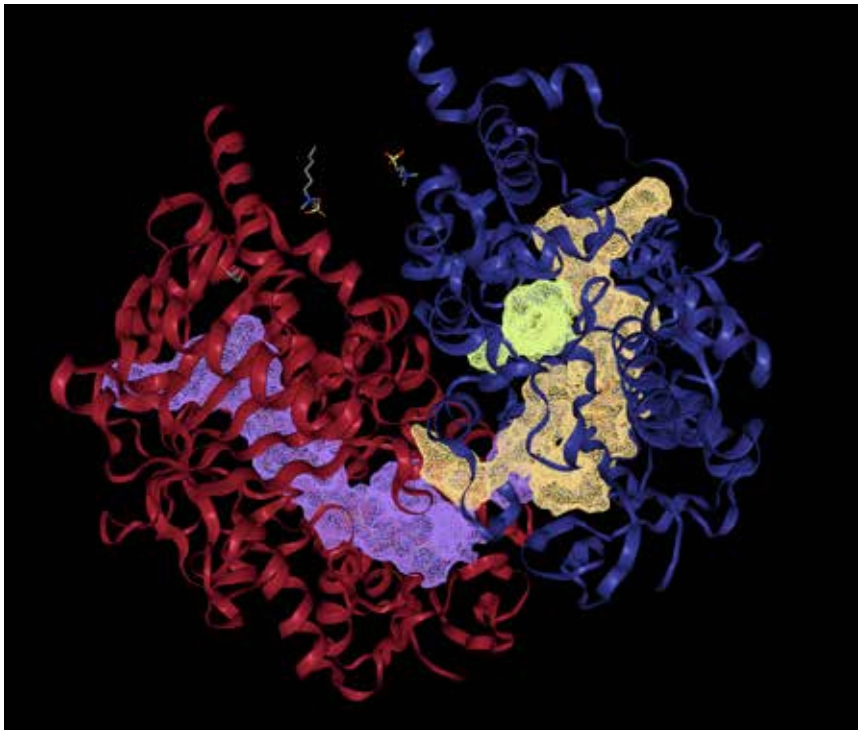

Figure 4. *All 17 potential binding sites identified by DoGSiteScorer, shown on the protein from two different angles*

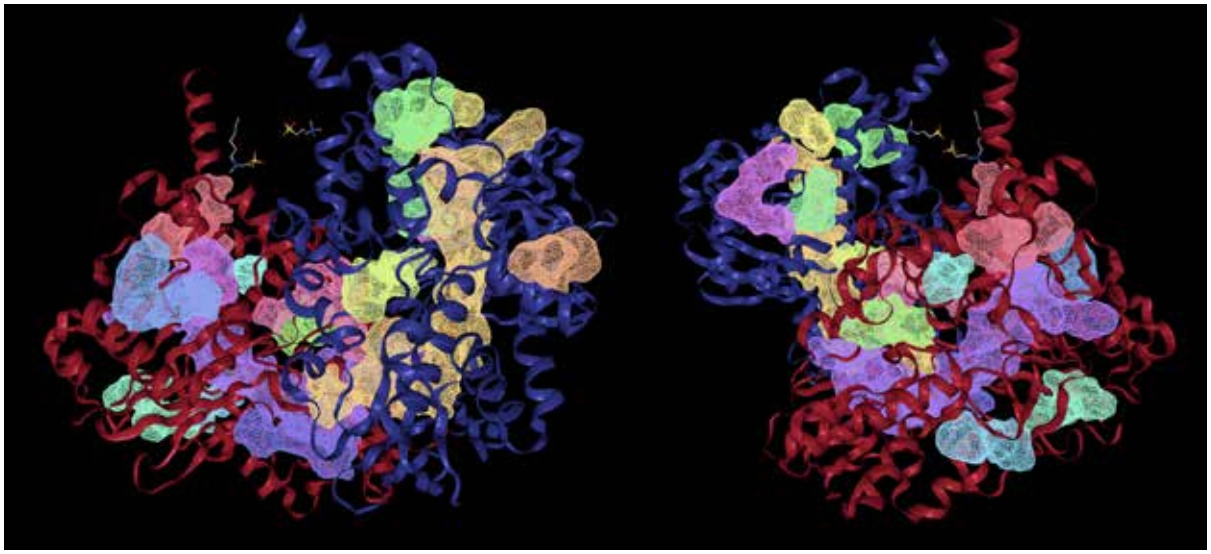

The energetic method, FTSite, was able to detect 3 possible binding sites, as shown in Figure 5. Two sites were on the side colored blue on DoGSiteScorer, and one site was on the side colored red (see above). Since FTSite is based on energetic rather than geometric favorability, it identified less potential binding sites.

Figure 5. *Results of the FTSite energetic binding site prediction for the MAO-B protein. The gray ribbon represents the protein structure, while the green, red, and purple represent potential binding sites.*

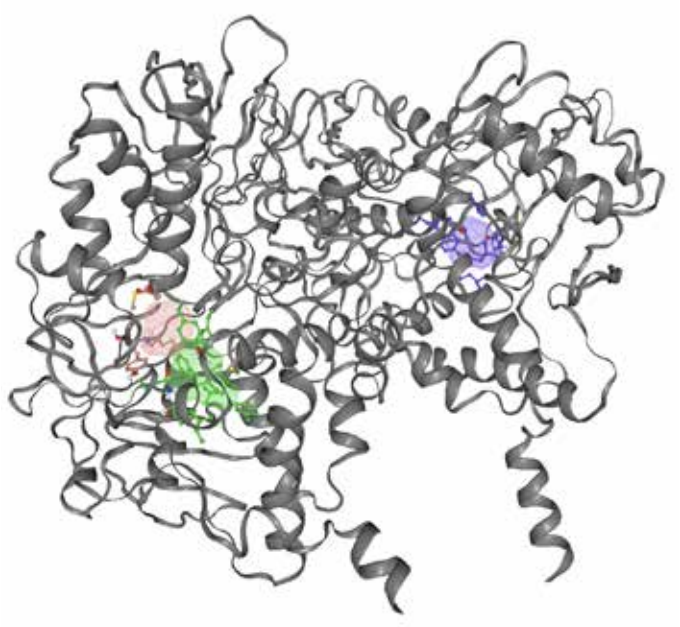

Finally, the machine learning method, P2Rank, was able to detect 12 binding sites, as shown in Table 2. Sites were ranked by score, and the data also included the number of residues for each site. The top two binding sites were consistent with DoGSiteScorer, as they were much larger than the rest. On PrankWeb, these two sites also had significantly higher scores and larger numbers of residues.

Table 2. *12 potential binding sites for the MAO-B protein detected by P2Rank, sorted by score.*

Rank sorted ascending	Score	# of residues
1	51.19	56
2	45.43	50
3	3.87	14
4	3.62	15
5	3.34	14
6	3.24	7
7	2.70	13
8	2.49	11
9	2.39	14
10	1.95	8
11	1.35	5
12	1.04	13

Figures 6 and 7 show various binding sites colored on the protein. Figure 6 shows the binding sites on the surface, and figure 7 shows them inside the MAO-B enzyme. As seen in figure 6, binding sites tended to be in concave pockets on the surface.

Figure 6. *Results of the P2Rank binding site prediction for the MAO-B protein. The gray represents the protein structure, while the colors represent potential binding sites. The protein is visualized by "surface" and the pockets are visualized by "surface (atoms)," shown from four different angles*

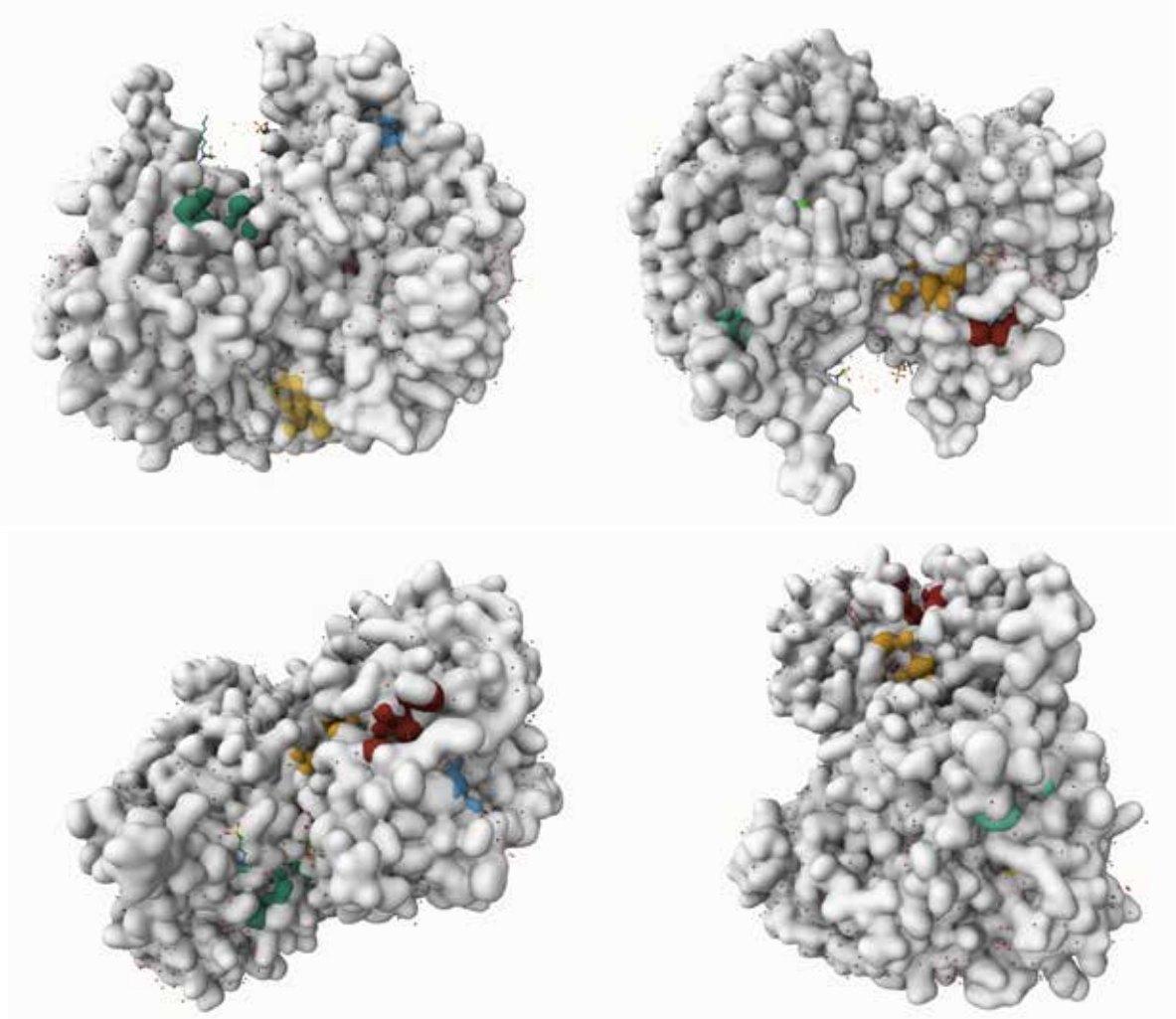

As shown in figure 7, the light yellow and red binding sites are significantly larger than the rest, suggesting that they might correspond to the sites P_0 and P_1 identified by DoGSiteScorer. These two sites also had distinctively higher scores of 51.19 and 45.43, compared with the rest of the sites with scores between 1 to 4.

Figure 7. Results of the P2Rank binding site prediction with the protein visualized by "cartoon" and the pockets visualized by "surface (residues)," shown from three different angles

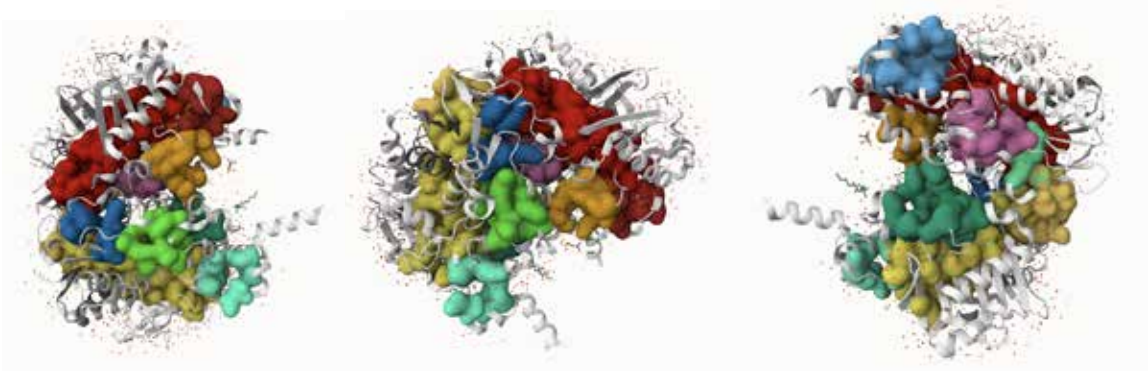

Pharmacophore Mapping

After potential binding sites were found, a pharmacophore map for the MAO-B protein that showed key features for binding was created. Instead of using the complete pharmacophore map for MAO-B, different combinations of pharmacophoric features were selected from Pharmit to create three maps with 6 to 9 features each, as shown in Figure 8. Each map focused on a distinctive aspect of MAO-B's pharmacophoric structure. The screening of the Enamine database for the first map only resulted in 3 potential drug candidates, so the second and third maps were added to find more compounds, producing 12 and 5 candidates respectively.

Figure 8. *Pharmit pharmacophore maps (1, 2, and 3 from left to right) generated from the MAO-B protein used to run virtual screening. Green spheres represent hydrophobic interactions, dark orange spheres represent negative ions, light orange spheres represent hydrogen acceptors, purple spheres represent aromatic interactions, and white spheres represent hydrogen donors*

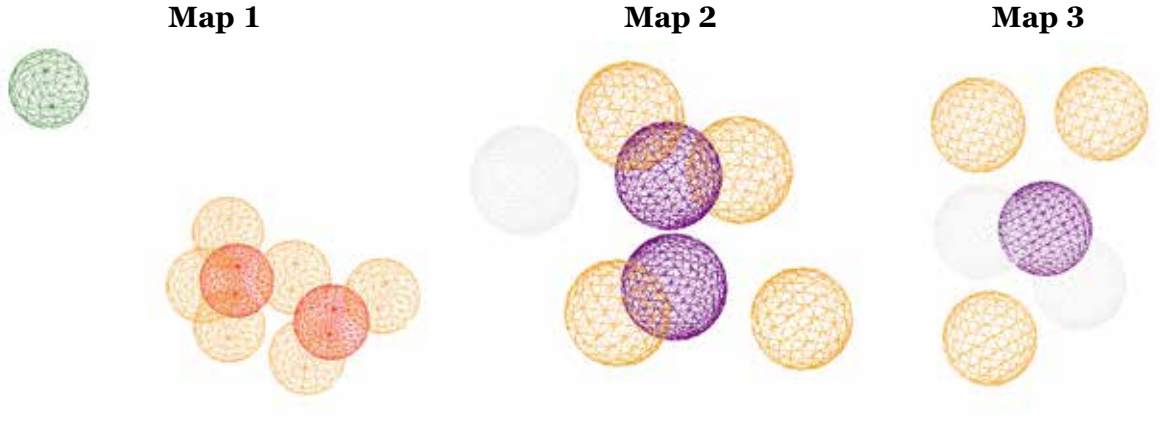

Tables 3–5, which summarize the 20 compounds identified from the pharmacophore mapping experiment, show that the features of the compounds align closely with those of the pharmacophore maps. A lower RMSD is better, as it means the compound deviates less from the map. Compounds yielded from the third pharmacophore map had the lowest RMSD scores, whereas those from the first map had the highest RMSD scores. As shown in Figure 8, Map 1 is larger and more spread out than Map 2 and Map 3. Although the compounds generated from Map 1 had higher RMSDs, they were still included to test if a larger map might lead to drugs with better docking capabilities despite having worse matches.

Table 3. *Name, root mean square deviation (RMSD), and structure of drug candidates detected by Pharmit's virtual screening of the Enamine database with the first pharmacophore map*

Name	Z4164535231	Z3810976496	Z3196311517
Structure		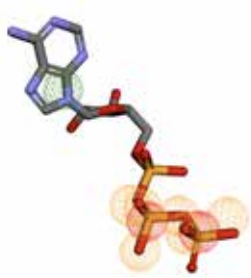	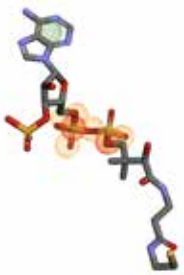
RMSD	0.440	0.460	0.512

Table 4. *Name, root mean square deviation (RMSD), and structure of drug candidates detected by Pharmit's virtual screening of the Enamine database with the second pharmacophore map*

Name	Z3810976496	Z2065614619	Z1082764572	Z1082764448
Structure			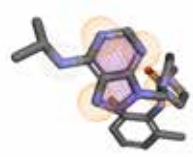	
RMSD	0.045	0.050	0.051	0.052
Name	Z1980993192	Z1980914346	Z56780075	Z1082766136
Structure			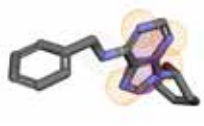	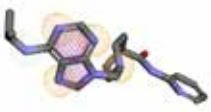
RMSD	0.056	0.061	0.062	0.063
Name	Z7911919636	Z4122876582	Z1980908378	Z4097793914
Structure				
RMSD	0.067	0.068	0.072	0.077

Table 5. *Name, root mean square deviation (RMSD), and structure of drug candidates detected by Pharmit's virtual screening of the Enamine database with the third pharmacophore map.*

Name	Z1201626990	Z1269216848	Z56790788	Z56758453	Z56776036
Structure					
RMSD	0.027	0.027	0.027	0.028	0.029

Molecular Docking

After molecular docking was assessed for each of the 20 compounds, most had a SwissParam score around –8, –9, or –10. During the docking simulation, the inhibitor was given the freedom to rotate around a defined box on the target and dock wherever possible. SwissDock then quantified the energy of

the interaction to determine how favorable binding would be. The top SwissParam score represented the Gibbs free energy (ΔG) of the best interaction in kilocalories per mole. The more negative the ΔG value, the more spontaneous the interaction, meaning that it consumed less energy and was more favorable. 10 compounds were selected by the most negative SwissParam score. The compound that performed the best was Z3196311517, followed by Z1082764448, the only two candidates that had SwissParam scores below –10. The SMILES of compound Z4097793914 was not accepted by SwissDock, likely due to the presence of boron, so it was removed from the screening. Compound Z3810976496 was found to be repeated, so its duplicate was taken out. The names and SwissParam scores of the top 10 compounds are bolded in Table 6 below. Although the three candidates identified from the first pharmacophore map had worse RMSD scores than the other seventeen, their SwissParam scores were all in the top 10 compounds for the molecular docking experiment. Compound Z3196311517 had the worst RMSD score, but it also had the most negative SwissParam score. The candidates identified from the third pharmacophore map generally had more positive SwissParam scores, likely due to their smaller size.

Table 6. *Results of molecular docking with SwissDock. In the residue interaction figures, the red ribbons represent the protein structure, the blue represents hydrogen bonds, and the yellow represents ionic interactions. The top 10 drug candidates are bolded*

Name	**Z4164535231**	**Z3810976496**	**Z3196311517**
SwissParam Score (kcal/mol)	**-9.8520**	**-9.9056**	**-10.7236**
Residue Interaction Figure	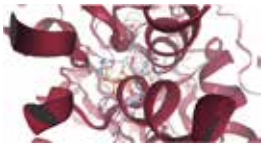		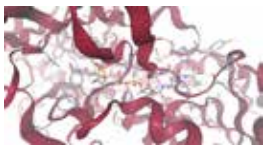
Name	**Z2065614619**	**Z1082764572**	**Z1082764448**
SwissParam Score (kcal/mol)	**-9.4043**	**-9.7102**	**-10.6647**
Residue Interaction Figure	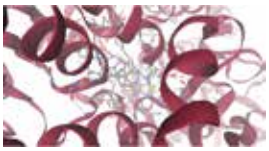	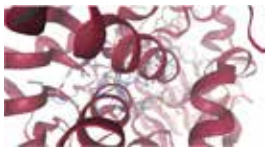	
Name	**Z1980993192**	**Z1980914346**	Z56780075
SwissParam Score (kcal/mol)	**-9.4726**	**-9.6217**	-8.5754
Residue Interaction Figure			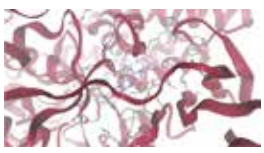
Name	**Z1082766136**	Z7911919636	Z4122876582
SwissParam Score (kcal/mol)	**-9.6193**	-8.2044	-8.9549
Residue Interaction Figure			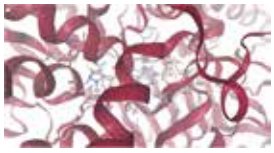

Name	Z1980908378	Z1201626990	Z1269216848
SwissParam Score (kcal/mol)	-8.7293	-6.4432	-6.7312
Residue Interaction Figure			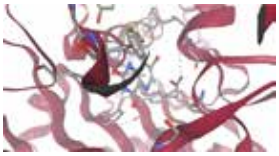
Name	**Z56790788**	**Z56758453**	**Z56776036**
SwissParam Score (kcal/mol)	-7.2137	-7.7093	**-9.7320**
Residue Interaction Figure	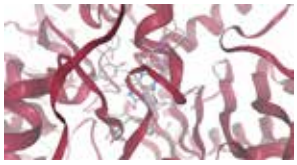	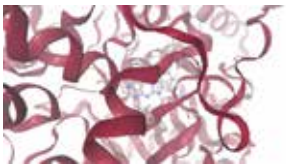	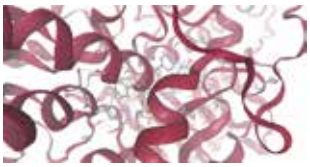

ADME Screening

After performing ADME screening on the top 10 remaining drug candidates, the top 7 were selected based on whether they satisfied Lipinski's Rule of Five, a set of four rules that predict oral bioavailability (Lipinski et al., 1997). The molecular weight (MW), number of hydrogen bond (H-bond) acceptors, number of H-bond donors, and consensus LogP value for each drug candidate were used to evaluate their adherence to Lipinski's Rule of Five. Although they were all in the top 10, none of the three drug candidates selected from the first pharmacophore map satisfied Lipinski's Rule of Five, likely due to their large size. As a result, compounds Z1082764448, Z56776036, Z1082764572, Z1980914346, Z1082766136, Z1980993192, and Z2065614619 were selected as the top 7 potential MAO-B inhibitors. Out of these seven, compound Z1082764448 had the most negative SwissParam score. Table 7 summarizes the results of the ADME screening.

Table 7. *Physicochemical properties of 10 potential MAO-B inhibitors identified by SwissADME, sorted by SwissParam score. Green highlighting indicates which compounds satisfy Lipinski's Rule of Five ("RoF" column)*

Molecule	Mol. Weight	# H-bond acceptors	# H-bond donors	LogP Value	RoF	Water Solubility	GI absorption	BBB permeant
Z3196311517	767.53 g/mol	19	9	-3.20	No	Highly soluble	Low	No
Z1082764448	479.97 g/mol	6	1	2.44	Yes	Moderately soluble	High	No
Z3810976496	551.14 g/mol	16	5	-9.72	No	Highly soluble	Low	No
Z4164535231	563.15 g/mol	17	7	-9.79	No	Highly soluble	Low	No
Z56776036	414.38 g/mol	7	3	1.52	Yes	Soluble	Low	No
Z1082764572	436.55 g/mol	6	2	2.05	Yes	Moderately Soluble	High	No
Z1980914346	443.50 g/mol	8	4	1.54	Yes	Moderately Soluble	High	No

Molecule	Mol. Weight	# H-bond acceptors	# H-bond donors	LogP Value	RoF	Water Solubility	GI absorption	BBB permeant
Z1082766136	394.47 g/mol	6	2	1.59	Yes	Soluble	High	No
Z1980993192	416.43 g/mol	9	4	0.35	Yes	Soluble	Low	No
Z2065614619	448.47 g/mol	7	5	1.26	Yes	Moderately Soluble	Low	No

Toxicity Screening

After the ADME screening, the remaining seven molecules were evaluated with ProTox-3.0 to determine their toxicity classification and LD50 value. Only compounds Z1082764448, Z56776036, and Z1980993192 were determined to be acceptably safe, as they had LD50 value above 400 mg/kg and toxicity classification above 3. The rest were deemed too toxic and eliminated from the screening. Results of the ProTox screening are shown in Table 8.

Table 8. *Toxicological properties of 7 potential MAO-B inhibitors identified by ProTox. Green highlighting indicates which compounds have both LD50 value > 400 mg/kg and toxicity classification > 3*

Name	LD50 (mg/kg)	Toxicity Classification
Z1082764448	2520	5
Z56776036	3000	5
Z1082764572	175	3
Z1980914346	29	2
Z1082766136	175	3
Z1980993192	1000	4
Z2065614619	13	2

For the remaining 3 drug candidates, the network chart and toxicity radar chart were assessed for additional toxicological analysis. The network chart shows the active (toxic) and inactive clusters, while the toxicity radar chart compares the active elements of the compound against their acceptable limits. Compounds passed the screening if they had at most one element exceeding average toxicity. Compound Z1082764448 exceeded the average toxicity for three elements (BBB by 3%, respiratory toxicity by 17%, and neurotoxicity by 7%), and compound Z1980993192 exceeded the average toxicity for one element (respiratory toxicity by 14%). As a result, only compounds Z56776036 and Z1980993192 passed the toxicity screening, although Z1980993192 has the limitation of its respiratory toxicity. Z56776036 is considered to be the safest of the top two molecules. Table 9 shows the network and toxicity radar chart results.

Table 9. *Network charts and toxicity radar charts generated by ProTox. The blue dots represent the toxicity of the compound for a specific element, while the orange dots represent the average toxicity of FDA approved drugs for that element*

Name	Network Chart	Toxicity Radar Chart
Z108...	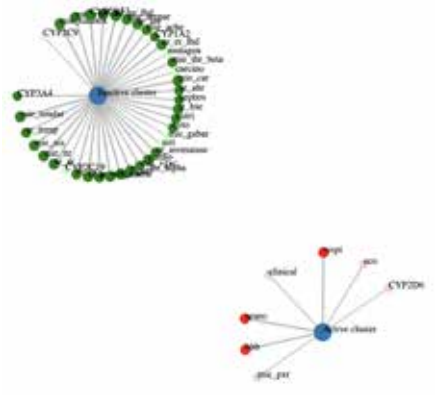	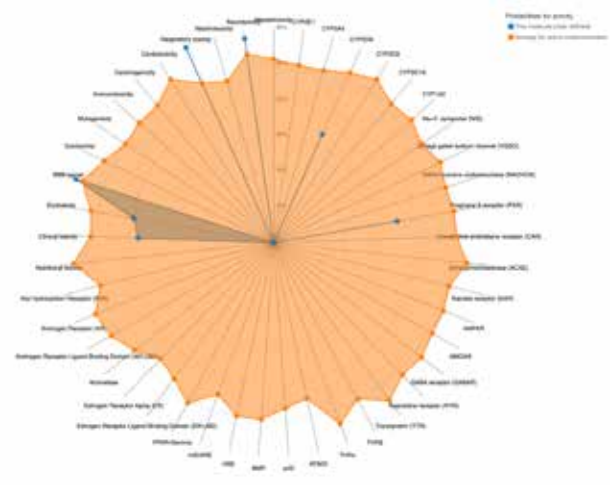
Z567...	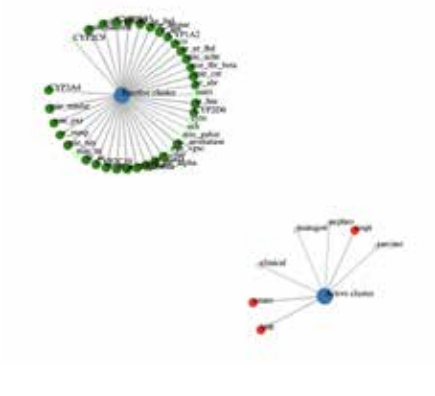	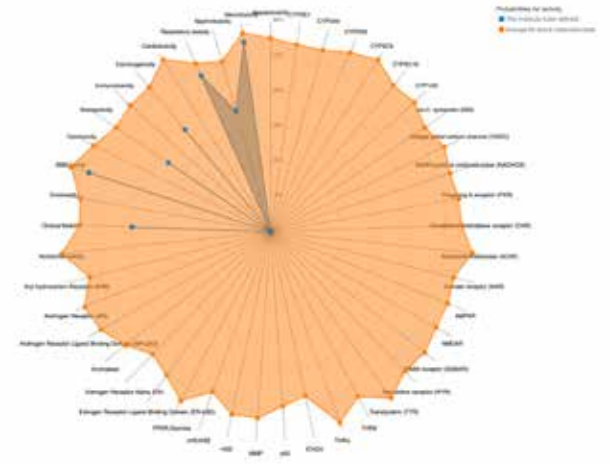
Z198...	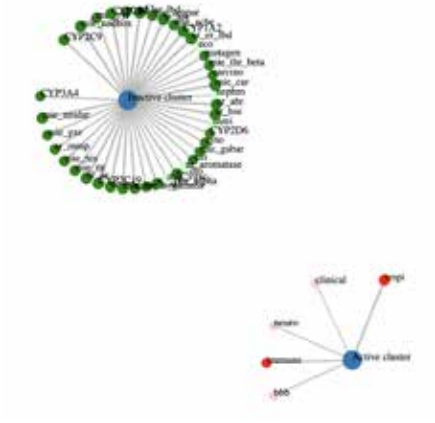	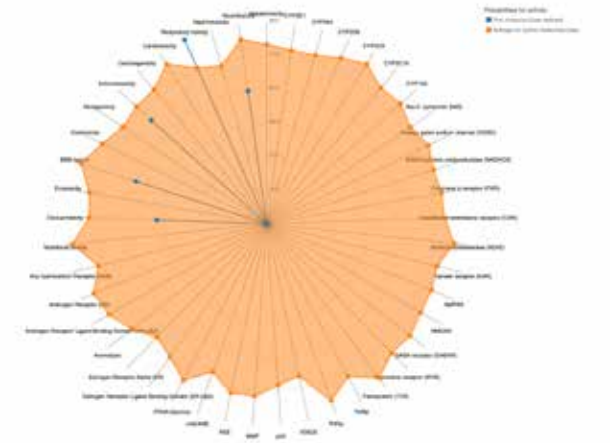

Conclusion

MAO-B is a critical therapeutic target for the neurodegenerative dementia Alzheimer's disease, as it causes Aβ plaques and neurofibrillary tangles, two key pathways to AD. This experiment focused on identifying novel MAO-B inhibitors with *in silico* screening to optimize for high binding affinity, druglike pharmacological properties, and low toxicity. Using computational methodology, po-

tential binding sites were identified on the MAO-B protein with DoGSiteScorer, FTSite, and PrankWeb. DoGSiteScorer was able to identify 38 binding sites, FTSite identified 3, and PrankWeb identified 12. Pharmacophore mapping was then used to screen the Enamine database, yielding 20 potential drug candidates. The 20 candidates were subsequently evaluated via molecular docking, and 10 were determined to be bioactive. SwissADME then identified that 7 of the top 10 adhered to Lipinski's Rule of Five. Finally, for toxicity prediction, ProTox was used to identify the 2 lead compounds with toxicity classification above 3 and at most one active element exceeding average toxicity. This experiment successfully discovered two promising MAO-B inhibitors as treatment for Alzheimer's disease. The final candidates, Z56776036 and Z1980993192, had excellent docking scores of –9.7320 and –9.4726 respectively, strong ADME profiles, and high LD50 values of 3000 mg/kg and 1000 mg/kg respectively. This study represents a valuable starting point for future work involving additional pharmacophoric screening targeting different areas of the MAO-B protein, as well as molecular docking for Chain A of the MAO-B enzyme with SwissDock. Further testing of the 2 lead compounds through *in vitro* or *in vivo* screening is needed to confirm this paper's findings, and additional *in silico* discovery of lead compounds can be conducted using the effective, low-cost methodology described in this paper.

References

Alzheimer's Association. (2024). Alzheimer's disease facts and figures. *Alzheimer's & Dementia*. Retrieved from https://www.alz.org/alzheimers-dementia/facts-figures

Balázs, N., Bereczki, D., & Kovács, T. (2021). Cholinesterase inhibitors and memantine for the treatment of Alzheimer and non-Alzheimer dementias. *Ideggyógyászati Szemle*, *74*(11–12), 379–387. Retrieved from https://doi.org/10.18071/isz.74.0379

Behl, T., et al. (2021). Role of monoamine oxidase activity in Alzheimer's disease: An insight into the therapeutic potential of inhibitors. *Molecules*, *26*(12), 3724. Retrieved from https://doi.org/10.3390/molecules26123724

Bugnon, M., et al. (2024). SwissDock 2024: Major enhancements for small-molecule docking with attracting cavities and AutoDock Vina. *Nucleic Acids Research*, *52*(W1). Retrieved from https://doi.org/10.1093/nar/gkae300

Chatzipieris, F. P., et al. (2024). New prospects in the inhibition of monoamine oxidase-B (MAO-B) utilizing propargylamine derivatives for the treatment of Alzheimer's disease. *ChemRxiv*. Retrieved from https://doi.org/10.26434/chemrxiv-2024-n73fc

da Costa, A. L. P., et al. (2024). In silico screening of monoamine oxidase B inhibitors for the treatment of central nervous system disorders. *Journal of the Brazilian Chemical Society*, *36*(4). Retrieved from https://doi.org/10.21577/0103–5053.20240192

Daina, A., et al. (2017). SwissADME: A free web tool to evaluate pharmacokinetics, drug-likeness, and medicinal chemistry friendliness of small molecules. *Scientific Reports*, *7*(1), 42717. Retrieved from https://doi.org/10.1038/srep42717

Doig, A. J. (2018). Positive feedback loops in Alzheimer's disease: The Alzheimer's feedback hypothesis. *Journal of Alzheimer's Disease*, *66*(1), 25–36. Retrieved from https://doi.org/10.3233/JAD-180583

Ebell, M. H., Barry, H. C., Baduni, K., & Grasso, G. (2024). Clinically important benefits and harms of monoclonal antibodies targeting amyloid for the treatment of Alzheimer disease: A systematic review and meta-analysis. *Annals of Family Medicine*, *22*(1), 50–62. Retrieved from https://doi.org/10.1370/afm.3050

GBD 2019 Dementia Forecasting Collaborators. (2022). Estimation of the global prevalence of dementia in 2019 and forecasted prevalence in 2050: An analysis for the Global Burden of Disease Study 2019. *The Lancet Public Health*, *7*(2), e105-e125. Retrieved from https://doi.org/10.1016/S2468–2667(21)00249–8

Grosdidier, A., Zoete, V., & Michielin, O. (2011). SwissDock, a protein–small molecule docking web service based on EADock DSS. *Nucleic Acids Research*, *39*(Suppl. 2), W270–W277. Retrieved from https://doi.org/10.1093/nar/gkr366

Hampel, H., et al. (2021). The amyloid-β pathway in Alzheimer's disease. *Molecular Psychiatry*, *26*(10), 5481–5503. Retrieved from https://doi.org/10.1038/s41380–021–01249–0

Jendele, L., Krivák, R., Škoda, P., Novotný, M., & Hoksza, D. (2019). PrankWeb: A web server for ligand binding site prediction and visualization. *Nucleic Acids Research*, *47*(W1), W345–W349. Retrieved from https://doi.org/10.1093/nar/gkz424

Krivák, R., & Hoksza, D. (2018). P2Rank: Machine learning-based tool for rapid and accurate prediction of ligand binding sites from protein structure. *Journal of Cheminformatics*, *10*(1). Retrieved from https://doi.org/10.1186/s13321–018–0285–8

Lipinski, C. A., et al. (1997). Experimental and computational approaches to estimate solubility and permeability in drug discovery and development settings. *Advanced Drug Delivery Reviews*, *23*(1–3), 3–25. Retrieved from https://doi.org/10.1016/S0169–409X(96)00423–1

Liew, Y., et al. (2023). Neuroinflammation: A common pathway in Alzheimer's disease and epilepsy. *Journal of Alzheimer's Disease*, *94*(Suppl. 1), S253–S265. Retrieved from https://doi.org/10.3233/JAD-230059

Ngan, C.-H., Hall, D. R., Zerbe, B., Grove, L. E., Kozakov, D., & Vajda, S. (2011). FTSite: High accuracy detection of ligand binding sites on unbound protein structures. *Bioinformatics*, *28*(2), 286–287. Retrieved from https://doi.org/10.1093/bioinformatics/btr651

Park, J.-H., et al. (2019). Newly developed reversible MAO-B inhibitor circumvents the shortcomings of irreversible inhibitors in Alzheimer's disease. *Science Advances*, *5*(3), eaav0316. Retrieved from https://doi.org/10.1126/sciadv.aav0316

Reis, J., et al. (2018). Tight-binding inhibition of human monoamine oxidase B by chromone analogs: A kinetic, crystallographic, and biological analysis. *Journal of Medicinal Chemistry*, *61*(9), 4203–4212. Retrieved from https://doi.org/10.1021/acs.jmedchem.8b00357

Sunseri, J., & Koes, D. R. (2016). Pharmit: Interactive exploration of chemical space. *Nucleic Acids Research*, *44*(W1), W442–W448. Retrieved from https://doi.org/10.1093/nar/gkw287

Svobodova, B., et al. (2023). Structure-guided design of N-methylpropargylamino-quinazoline derivatives as multipotent agents for the treatment of Alzheimer's disease. *International Journal of Molecular Sciences*, *24*(11), 9124. Retrieved from https://doi.org/10.3390/ijms24119124

Volkamer, A., Kuhn, D., Grombacher, T., Rippmann, F., & Rarey, M. (2012). Combining global and local measures for structure-based druggability predictions. *Journal of Chemical Information and Modeling*, *52*(2), 360–372. Retrieved from https://doi.org/10.1021/ci200454v

Zhang, J., Zhang, Y., Wang, J., Xia, Y., Zhang, J., & Chen, L. (2024). Recent advances in Alzheimer's disease: Mechanisms, clinical trials, and new drug development strategies. *Signal Transduction and Targeted Therapy*, *9*(1), Article 191. Retrieved from https://doi.org/10.1038/s41392–024–01911–3

Zuliani, G., Zuin, M., Romagnoli, T., Polastri, M., Cervellati, C., & Brombo, G. (2024). Acetylcholinesterase inhibitors reconsidered: A narrative review of post-marketing studies on Alzheimer's disease. *Aging Clinical and Experimental Research*, *36*(1), 1–10. Retrieved from https://doi.org/10.1007/s40520–023–02675–6

submitted 08.12.2025;
accepted for publication 22.12.2025;
published 30.12.2025

Contact: iamroryhu@gmail.com